

CLIFF-LEARNING

Tony T. Wang¹ Igor Zablotski¹² Nir Shavit¹³ Jonathan S. Rosenfeld¹
 {ttw, shanir, jonsr}@csail.mit.edu igor.zablotski@gmail.com
¹MIT ²Mysten Labs ³Neural Magic

ABSTRACT

We study the data-scaling of transfer learning from foundation models in the low-downstream-data regime. We observe an intriguing phenomenon which we call *cliff-learning*. Cliff-learning refers to regions of data-scaling laws where performance improves at a faster than power law rate (i.e. regions of concavity on a log-log scaling plot). We conduct an in-depth investigation of foundation-model cliff-learning and study toy models of the phenomenon. We observe that the degree of cliff-learning reflects the degree of compatibility between the priors of a learning algorithm and the task being learned.

1 INTRODUCTION

The use of pre-trained models as a foundation (Bommasani et al., 2021) for learning has resulted in groundbreaking advances in AI. For example, ChatGPT is a finetuned version of GPT-3 (Brown et al., 2020), and Stable Diffusion (Rombach et al., 2022) is built on top of CLIP-type models (Radford et al., 2021). In addition to enabling new capabilities, transfer learning on top of foundation models enables deep-learning to function in scenarios where training data is limited.

One way to evaluate the effectiveness of transfer-learning is to look at its data-scaling behavior: how fast does test error decay when we increase the amount of (downstream) training data? Hernandez et al. (2021) finds that when the number of training samples n is large (Appendix A), transfer-learning test error decays as a power law in n :

$$\mathbb{E}_{D \text{ an i.i.d. dataset of size } n} [\text{test-error}(\text{model trained on } D)] = A \times n^{-\alpha} + E. \quad (1.1)$$

This corroborates a large body of work that finds such power laws are very accurate models of data-scaling for neural networks in the large- n regime (Seung et al., 1992; Hestness et al., 2017; Rosenfeld et al., 2019; Kaplan et al., 2020; Hoffmann et al., 2022).

Yet, little is known about the low-data regime. We discover that power laws are not an accurate model of transfer learning data-scaling in the low-data regime; instead, performance often improves at a faster than power law rate. On a log-log plot, this shows up as a concave scaling-law (Appendix B). We dub such regions of concavity *cliff-learning* regions. These regions are arguably the most interesting parts of the data-scaling domain, since they have the highest “return on data”.

In Section 2, we investigate cliff-learning with foundation models. In Section 3, we develop toy models for cliff-learning. We discuss implications and open questions in Section 4.

2 FOUNDATION MODEL TRANSFER LEARNING

Figure 2.1 shows a prototypical example of transfer learning cliff: finetuning a LAION-CLIP (Schuhmann et al., 2022) linear probe on CIFAR-10 produces an initial cliff-learning phase that lasts until the model achieves human parity. This is $1000\times$ more efficient than learning from scratch.¹

Figure 2.1 also compares finetuning to data-pruning, which was explored as a method for beating power-law scaling in Sorscher et al. (2022b). We find that data-pruning alone does not perform meaningfully better than training from scratch. Data-pruning combined with transfer learning

¹In Appendix D.1, we show that linear probe finetuning does not always result in cliff-learning; sometimes, full model finetuning is needed.

demonstrates stronger signatures of cliff-learning², but is outperformed by a linear probe on top of a stronger foundation model.

In Figure 2.2, we compare different methods of finetuning for CLIP models of varying quality. The asymptotic behavior of different finetuning methods can be grouped into a few different categories: linear-probes plateau, full-model finetuning shares the asymptotics of from-scratch training, and deeper fully-connected probes share the same asymptotics as k -NN probes. However, these asymptotics are only similar in slope; their intercepts are different due differences in transient cliff-learning dynamics. In other words, the quality of a foundation model primarily influences data-scaling in the regime of cliff-learning, higher quality foundation models cliffing more aggressively, and all models share the same asymptotic behaviors in the large- n regime. We conjecture that shared asymptotics arise due to shared mechanisms of learning.

²For more commentary on data-pruning, see Appendix A.

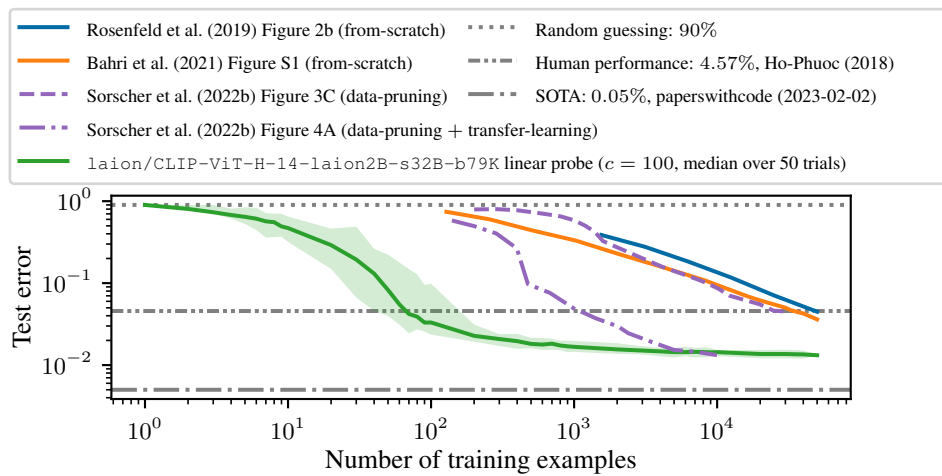


Figure 2.1: Data-scaling of transfer learning, data-pruning, and from-scratch learning on CIFAR-10. The shaded region represents the full range of measured values across all trials. For Sorscher et al. (2022b), Pareto-optimal curves across different pruning fractions are plotted.

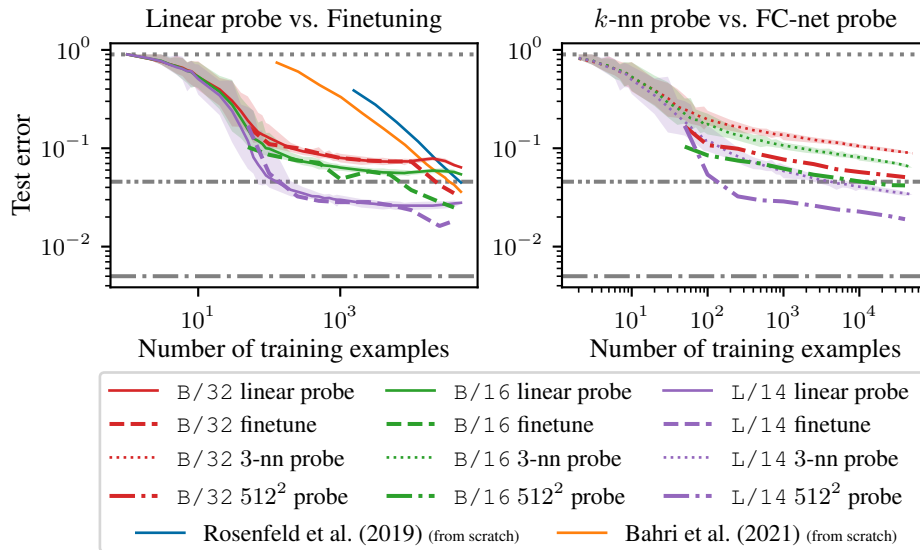


Figure 2.2: Data-scaling of different finetuning methods on CIFAR-10 for three OpenAI CLIP models of increasing quality: B/32 < B/16 < L/14. The method “finetune” consisted of finetuning all models parameters after the final readout layer was initialized to the optimal linear probe. The 512² probe was a two layer fully connected ReLU probe of width 512. Shaded regions are for 50 trials, with medians marked. See Figures D.2 and D.3 for related results.

3 TOY MODELS OF CLIFF-LEARNING

We now study some toy-models of cliff-learning. Our toy-models have a unifying principle: the more the priors of a learning algorithm match the task being learned, the more cliff-learning occurs.

3.1 CLIFF-LEARNING IN LINEAR REGRESSION

Say we want to learn a linear function $f(x) = v^\top x$ in d -dimensions (i.e. $v, x \in \mathbb{R}^d$) from training data $\{(x_i, y_i)\}_{i=1}^n$, where the $y_i = f(x_i) + \mathcal{N}(0, \sigma^2)$ are noisy observations.

When $n < d$, there are infinitely many linear functions that perfectly fit the training data. In this regime, it is hopeless to achieve small error. However when $n \geq d$ and $\sigma = 0$, we can perfectly³ learn f via the following least-squares algorithm:

$$\hat{f}(x) = \hat{v}^\top x, \quad \hat{v} = \arg \min_w \sum_{i=1}^n (w^\top x_i - y_i)^2. \quad (3.1)$$

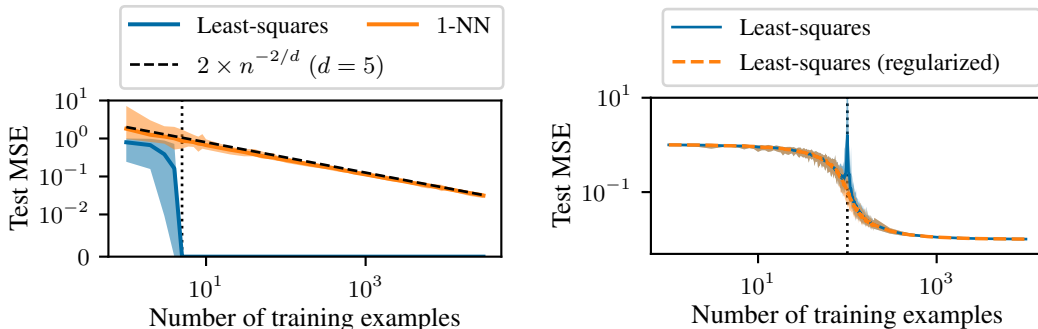
This least-squares estimator demonstrates cliff-learning – when the training dataset is at least of size d (the critical threshold), test-error instantly drops to zero. This cliff is shown in Figure 3.1a, where it is contrasted against the power law scaling of a nearest-neighbor estimator. The reason our least-squares estimator demonstrates cliff-learning while a nearest-neighbor estimator does not is because our least-squares estimator forces the learnt estimator to be linear, a prior that matches the task being learned.

When $\sigma > 0$, the least-squares estimator in Equation (3.1) can suffer from double descent, but adding a regularization term $\lambda \|v\|_2^2$ to its objective recovers a softer-form of cliff-learning (Figure 3.1b).

3.2 CLIFF-LEARNING IN BINARY GAUSSIAN CLASSIFICATION

In Appendix F, we study a binary Gaussian classification problem that exhibits cliff-learning. We are able to work out the exact functional form of cliff-learning in this case (Equation (F.5)), and the resulting cliff-learning curves (Figure F.1) look very similar to Figure 3.1b.

³Also assuming the x_i are linearly independent, which is almost surely true if for example the x_i are sampled i.i.d. from $\mathcal{N}(0, I_d)$.



(a) Data-scaling curves on a noiseless linear regression task with $d = 5$ and $\|v\|_2 = 1$. The y -axis is on a linear scale below 10^{-2} .

(b) Data-scaling curves on a noisy linear regression task with $d = 100$, $\|v\|_2 = 1$, and $\sigma = 0.1$. The regularization strength is $\lambda = d\sigma^2/\|v\|_2^2 = 1$.

Figure 3.1: Cliffs arise around the critical threshold $n = d$ (dotted vertical lines) for the linear regression toy problem from Section 3.1. We sample $x_i \stackrel{\text{i.i.d.}}{\sim} \mathcal{N}(0, I_d)$. 50 random trials are visualized, with shading denoting range and solid lines denoting medians. **(a)** On noiseless linear regression, a least-squares estimator exhibits a sharp cliff at d samples, while a nearest neighbor estimator exhibits power law scaling with exponent $-2/d$ (as suggested by theory, c.f. Györfi et al. (2002) Theorem 6.2). **(b)** In the noisy setting, regularized least-squares exhibits a soft cliff around d samples, and regularization is needed to avoid double-descent. We set the regularization strength λ to the “optimal” value c.f. Nakkiran et al. (2020).

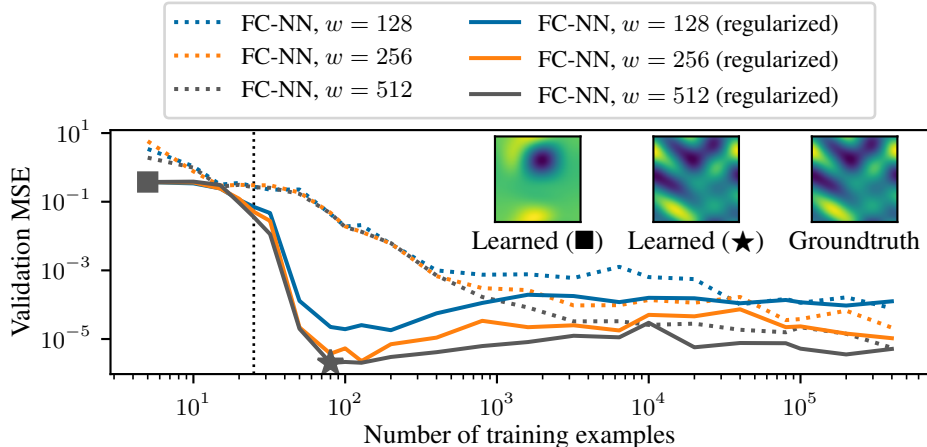


Figure 3.2: Data-scaling curves for a fully connected ReLU network with 3 hidden layers trained using Adam to learn a 2D harmonic function from Section 3.3 with bandlimit $B = 2$ (visualized in the top right). Without regularization, the data-scaling laws follow a power law trend, plateauing at a level governed by network size. With bandwidth regularization, we get cliff-learning around the theoretical limit of $n = (2B+1)^2$ (vertical dotted line). Why our method has slightly non-monotonic scaling after the initial cliff is an open question.

3.3 CLIFF-LEARNING AND REGULARIZATION

In this section, we train neural networks to learn 2D bandlimited periodic functions of the form

$$h(x) = \sum_{a,b \in \{-B, \dots, B\}} \alpha_{ij} \cos(2\pi(ax_1 + bx_2)) + \beta_{ij} \sin(2\pi(ax_1 + bx_2)), \quad (3.2)$$

where $h : [0, 1]^2 \rightarrow \mathbb{R}$. We train our networks to minimize the mean-squared error on datasets $\{(x_i, h(x_i))\}_{i=1}^n$ where the x_i 's are sampled i.i.d. from $\text{Unif}([0, 1]^2)$.

When trained to minimize MSE loss, our networks obey power-law loss scaling. However, in principle, sampling theory tells us that we can reconstruct h perfectly from just $(2B+1)^2$ distinct samples. We show in Figure 3.2 it is possible to make neural networks cliff have a soft-cliff at this threshold by regularizing their high-frequency components (see Appendix E).

Regularization can be considered the dual form of a prior. The fact that we get cliff-learning with regularization, and power-law scaling without regularization, supports our view that cliff-learning arises from prior-task compatibility.

4 DISCUSSION AND OPEN QUESTIONS

Our toy models in Section 3 suggest stronger cliffs arise from better prior-task compatibility. This corroborates our findings in Section 2 – we find that the quality of a foundation model (aka the quality of a learned prior) primarily manifests in data-scaling via the initial cliff-learning regime. In the large- n regime, foundation models of different qualities all scale as power laws with similar α s c.f. Equation (1.1), but different quality models have different A s and E s due to different amounts of cliff-learning.

Finally, we present some open questions:

1. In Section 3, we conjectured that when two different types of training methods share the same data-scaling asymptotics, they share similar “mechanisms” of learning. For example, if a learning algorithm \mathcal{A} has the same asymptotics as a nearest-neighbors method, does this imply \mathcal{A} is “memorizing” the training data? What other “mechanisms” are there?
2. We showed that cliff-learning can be achieved by finetuning foundation models. However, these large foundation models generally follow power law scaling in compute, parameters, and data. Is it possible for large foundation models to exhibit strong cliff-learning when trained from scratch? Or is there some sort of conservation principle that says a large amount of data is required somewhere in the learning pipeline?

REFERENCES

- Sanjeev Arora, Hrishikesh Khandeparkar, Mikhail Khodak, Orestis Plevrakis, and Nikunj Saunshi. A theoretical analysis of contrastive unsupervised representation learning. *arXiv preprint arXiv:1902.09229*, 2019.
- Yasaman Bahri, Ethan Dyer, Jared Kaplan, Jaehoon Lee, and Utkarsh Sharma. Explaining neural scaling laws. *arXiv preprint arXiv:2102.06701*, 2021.
- Hangbo Bao, Li Dong, Songhao Piao, and Furu Wei. Beit: Bert pre-training of image transformers. *arXiv preprint arXiv:2106.08254*, 2021.
- Lukas Biewald. Experiment tracking with weights and biases, 2020. URL <https://www.wandb.com/>. Software available from wandb.com.
- Rishi Bommasani, Drew A Hudson, Ehsan Adeli, Russ Altman, Simran Arora, Sydney von Arx, Michael S Bernstein, Jeannette Bohg, Antoine Bosselut, Emma Brunskill, et al. On the opportunities and risks of foundation models. *arXiv preprint arXiv:2108.07258*, 2021.
- Tom Brown, Benjamin Mann, Nick Ryder, Melanie Subbiah, Jared D Kaplan, Prafulla Dhariwal, Arvind Neelakantan, Pranav Shyam, Girish Sastry, Amanda Askell, et al. Language models are few-shot learners. *Advances in neural information processing systems*, 33:1877–1901, 2020.
- László Györfi, Michael Köhler, Adam Krzyżak, and Harro Walk. *A distribution-free theory of nonparametric regression*, volume 1. Springer, 2002.
- Danny Hernandez, Jared Kaplan, Tom Henighan, and Sam McCandlish. Scaling laws for transfer. *arXiv preprint arXiv:2102.01293*, 2021.
- Joel Hestness, Sharan Narang, Newsha Ardalani, Gregory Diamos, Heewoo Jun, Hassan Kianinejad, Md Patwary, Mostofa Ali, Yang Yang, and Yanqi Zhou. Deep learning scaling is predictable, empirically. *arXiv preprint arXiv:1712.00409*, 2017.
- Tien Ho-Phuoc. Cifar10 to compare visual recognition performance between deep neural networks and humans. *arXiv preprint arXiv:1811.07270*, 2018.
- Jordan Hoffmann, Sebastian Borgeaud, Arthur Mensch, Elena Buchatskaya, Trevor Cai, Eliza Rutherford, Diego de Las Casas, Lisa Anne Hendricks, Johannes Welbl, Aidan Clark, et al. Training compute-optimal large language models. *arXiv preprint arXiv:2203.15556*, 2022.
- Jeremy Howard. Imagenet, 2022. URL <https://github.com/fastai/imagenette/>.
- Jared Kaplan, Sam McCandlish, Tom Henighan, Tom B Brown, Benjamin Chess, Rewon Child, Scott Gray, Alec Radford, Jeffrey Wu, and Dario Amodei. Scaling laws for neural language models. *arXiv preprint arXiv:2001.08361*, 2020.
- Diederik P Kingma and Jimmy Ba. Adam: A method for stochastic optimization. *arXiv preprint arXiv:1412.6980*, 2014.
- Preetum Nakkiran, Prayaag Venkat, Sham Kakade, and Tengyu Ma. Optimal regularization can mitigate double descent. *arXiv preprint arXiv:2003.018957*, 2020.
- Yuval Netzer, Tao Wang, Adam Coates, Alessandro Bissacco, Bo Wu, and Andrew Y. Ng. Reading digits in natural images with unsupervised feature learning. In *NIPS Workshop on Deep Learning and Unsupervised Feature Learning 2011*, 2011. URL http://ufldl.stanford.edu/housenumbers/nips2011_housenumbers.pdf.
- nostalgebraist. chinchilla’s wild implications. AI Alignment Forum, 2022. URL <https://www.alignmentforum.org/posts/6Fpvch8RR29qLEWNH/chinchilla-s-wild-implications>.
- F. Pedregosa, G. Varoquaux, A. Gramfort, V. Michel, B. Thirion, O. Grisel, M. Blondel, P. Prettenhofer, R. Weiss, V. Dubourg, J. Vanderplas, A. Passos, D. Cournapeau, M. Brucher, M. Perrot, and E. Duchesnay. Scikit-learn: Machine learning in Python. *Journal of Machine Learning Research*, 12:2825–2830, 2011.

- Alec Radford, Jong Wook Kim, Chris Hallacy, Aditya Ramesh, Gabriel Goh, Sandhini Agarwal, Girish Sastry, Amanda Askell, Pamela Mishkin, Jack Clark, et al. Learning transferable visual models from natural language supervision. In *International conference on machine learning*, pp. 8748–8763. PMLR, 2021.
- Robin Rombach, Andreas Blattmann, Dominik Lorenz, Patrick Esser, and Björn Ommer. High-resolution image synthesis with latent diffusion models. In *Proceedings of the IEEE/CVF Conference on Computer Vision and Pattern Recognition*, pp. 10684–10695, 2022.
- Jonathan S Rosenfeld, Amir Rosenfeld, Yonatan Belinkov, and Nir Shavit. A constructive prediction of the generalization error across scales. *arXiv preprint arXiv:1909.12673*, 2019.
- Christoph Schuhmann, Romain Beaumont, Richard Vencu, Cade Gordon, Ross Wightman, Mehdi Cherti, Theo Coombes, Aarush Katta, Clayton Mullis, Mitchell Wortsman, et al. Laion-5b: An open large-scale dataset for training next generation image-text models. *arXiv preprint arXiv:2210.08402*, 2022.
- Hyunjune Sebastian Seung, Haim Sompolinsky, and Naftali Tishby. Statistical mechanics of learning from examples. *Physical review A*, 45(8):6056, 1992.
- Ben Sorscher, Surya Ganguli, and Haim Sompolinsky. Neural representational geometry underlies few-shot concept learning. *Proceedings of the National Academy of Sciences*, 119(43): e2200800119, 2022a.
- Ben Sorscher, Robert Geirhos, Shashank Shekhar, Surya Ganguli, and Ari S Morcos. Beyond neural scaling laws: beating power law scaling via data pruning. *arXiv preprint arXiv:2206.14486*, 2022b.
- Tom Viering and Marco Loog. The shape of learning curves: a review. *arXiv preprint arXiv:2103.10948*, 2021.

APPENDIX

A RELATED WORK

Hernandez et al. (2021) studies scaling laws for transfer learning and concludes that power law data-scaling holds for transfer learning. However the experiments in Hernandez et al. (2021) are conducted exclusively in the large- n regime (even the smallest experiments use $> 3 \times 10^5$ characters of downstream text data). In our experiments, we observed that cliff-learning is a transient phenomenon and that data-scaling reverts to a power law in the large- n regime. We believe the absence of cliff-like behavior in Hernandez et al. (2021) is caused by working in a large- n regime where cliff-learning does not apply.

Arora et al. (2019) proposes a theoretical model that explains why contrastive-learning produces representations that support well-performing linear probes. However, Arora et al. (2019) provides limited analysis of the data-efficiency of learning such probes, and their theoretical model is also not fully applicable to CLIP-style models.

Sorscher et al. (2022a) studies the data-scaling of linear probes for foundation models and macaque inferotemporal cortex representations.

While previous work (Hestness et al., 2017; Rosenfeld et al., 2019) has also found that power laws do not hold in the low-data regime, our work is the first to examine the transfer learning setting in this regime, and is the first to identify the cliff-learning phenomenon.

Sorscher et al. (2022b) proposes data pruning as a method for beating power law scaling. However, while data-pruning reduces the amount of data that is trained on, it still requires a large corpus of data on which pruning is performed. Thus data-pruning improves compute scaling but does not reduce the net amount of data required to reach a given loss.⁴ Moreover, the empirical performance of the data-pruning techniques demonstrated Sorscher et al. (2022b) are greatly outperformed by the cliff-learning we observe for foundational model transfer learning (Figure 2.1). Nonetheless, the ideas in Sorscher et al. (2022b) could plausibly be extended into the active-learning or reinforcement learning setting, where intelligent selection of data / environment exploration could yield true improvements in data-scaling.

Finally Viering & Loog (2021) surveys prior work on cliff-learning⁵ for both humans and machines. However, none of the surveyed works demonstrate cliff-learning in the context of deep learning. Compared to Viering & Loog (2021) our main contribution is to provide a unifying framework of prior/task compatibility to explain cliff-learning, and to demonstrate that it can be achieved with deep-neural networks in practical scenarios via transfer learning on top of foundation models (Bommasani et al., 2021).

B CONCAVITY ON A LOG-LOG PLOT

We provide a short proof that any scaling law of the form $f(n) = A \times n^{-\alpha} + E$ is non-concave when plotted on log-log scale. Thus, any scaling law which is concave must (locally) scale faster than any power law.

Proposition B.1. *For $A, \alpha, E \geq 0$, a power law of the form $f(n) = A \times n^{-\alpha} + E$ is non-concave when plotted on a log-log scale.*

Proof. If A or α are zero, $f(n)$ is a constant and non-concave. Otherwise,

$$\frac{\partial^2}{\partial x^2} \log(f(e^x)) = \log(A \times (e^x)^{-\alpha} + E) = \frac{\alpha^2 A E e^{\alpha x}}{(A + E e^{\alpha x})^2} \geq 0. \quad \square$$

⁴For example, data pruning on its own can not address the issue of large language models requiring more data than is easily obtainable from the internet, c.f. nostalgebraist (2022).

⁵Viering & Loog (2021) refers to cliff-learning as a “phase-transition” in data-scaling.

C EXPERIMENTAL DETAILS

- Linear probes were trained using scikit-learn (Pedregosa et al., 2011) with $C = 100$ as the regularization parameter (Figures 2.1, 2.2 and D.1).
- With the exception of linear probes, we used the Adam optimizer (Kingma & Ba, 2014) to train / finetune neural networks.
- For full model finetuning, we used a validation set for early stopping, which strictly speaking should be counted as part of the training dataset. We choose to omit the validation set from the training dataset size since we believe it is possible to find a smarter mechanism for model selection / early stopping that does not require a large validation set. On CIFAR-10 and SVHN (Figures 2.2 and D.1), the validation set was of size 10^4 and this set was used both for early stopping and for checkpoint selection (the checkpoint with the lowest validation loss was selected). On the harmonic function learning task (Figure 3.2), a validation set of size 512 was used for early-stopping, and the final checkpoint right before stopping was selected for final evaluation. The same validation set was also used as the test set.
- Curves for the cited papers are extracted from original publication figures via WebPlotDigitizer (Figures 2.1, 2.2 and D.1).
- Data-scaling experimental data was tracked using Weights & Biases (Biewald, 2020).

D MORE FOUNDATION MODEL TRANSFER LEARNING RESULTS

D.1 FOUNDATION MODELS DO NOT ALWAYS YIELD CLIFF-LEARNING

We show in Figures D.1 and D.2 that foundation-model transfer learning does not always yield substantial cliff-learning.

D.2 MORE LINEAR PROBE DATA-SCALING

We give plot more data-scaling laws for foundation model linear probes in Figure D.3.

E MONTE-CARLO BANDWIDTH REGULARIZATION

In this section, we describe how we can regularize the high-frequency components of a function $f_\theta : [0, 1]^d \rightarrow \mathbb{R}$.

If a function f_θ has bandlimit B , this means there exists coefficients a_v and b_v such that

$$f_\theta(x) = \sum_{v \in \text{nneg}([\pm B]^d)} a_v \cos(2\pi v^\top x) + \sum_{v \in \text{nneg}([\pm B]^d) - \{\mathbf{0}\}} b_v \sin(2\pi v^\top x),$$

where $[\pm B] \triangleq \{-B, \dots, 0, \dots, B\}$ and nneg is defined as

```
def nneg(vs: list[np.ndarray[d]]) -> list[np.ndarray[d]]:
    def _include(v: np.ndarray[d]) -> bool:
        nonzero_coords = v[v != 0]
        if len(nonzero_coords) == 0:
            return True
        return nonzero_coords[0] > 0
    return [v for v in vs if _include(v)]
```

Let S_B denote the subspace of real-valued functions over $[0, 1]^d$ that is spanned by the orthonormal basis

$$\Phi_B \triangleq \{\cos(2\pi v^\top x) \mid v \in \text{nneg}([\pm B]^d)\} \sqcup \{\sin(2\pi v^\top x) \mid v \in \text{nneg}([\pm B]^d) - \{\mathbf{0}\}\}.$$

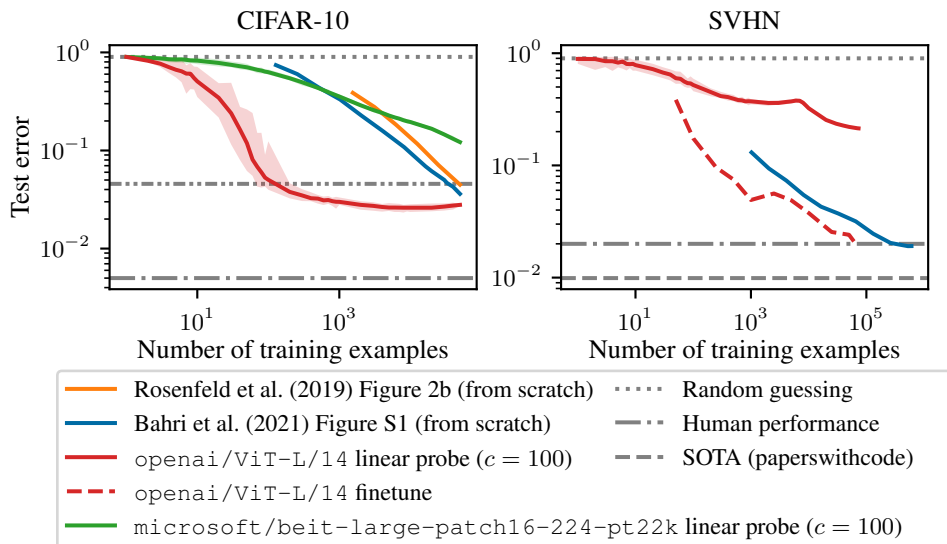


Figure D.1: Data-scaling laws for deep neural networks on two standard image classification benchmarks. Some but not all of the laws exhibit cliff-scaling. Shading captures the range of measured values across 50 different trials, and solid lines denote the median over trials. Humans achieve 4.57% error on CIFAR-10 (Ho-Phuoc, 2018) and 2% error on SVHN (Netzer et al., 2011). **Left:** A ViT CLIP model has a large region of cliff-learning, spanning from random-guessing to human parity. However, foundation model finetuning does not always result in a cliff, as demonstrated by a BeIT linear probe (Bao et al., 2021). **Right:** While a CLIP linear-probe aggressively cliffs on CIFAR10, it behaves much closer to a power-law on SVHN. Finetuning the whole CLIP model yields a curve with similar asymptotics to from-scratch learning, though we can infer the finetuning curve must cliff more in the small- n regime (since error cannot exceed 100%).

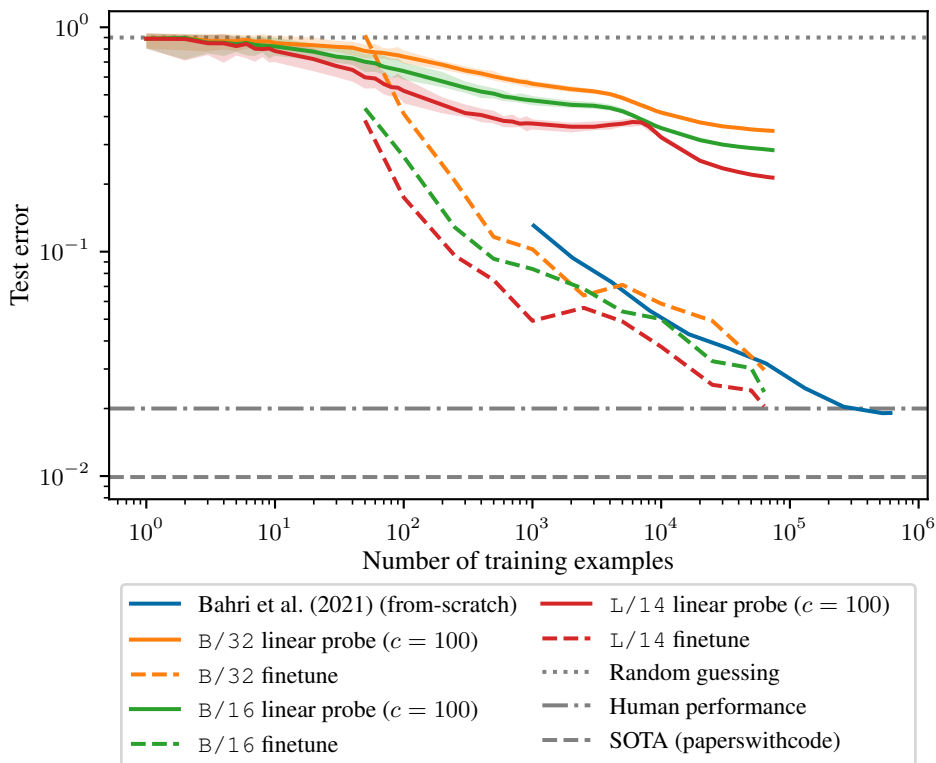


Figure D.2: Data-scaling of different finetuning methods on SVHN for three OpenAI CLIP models of increasing quality: $B/32 < B/16 < L/14$.

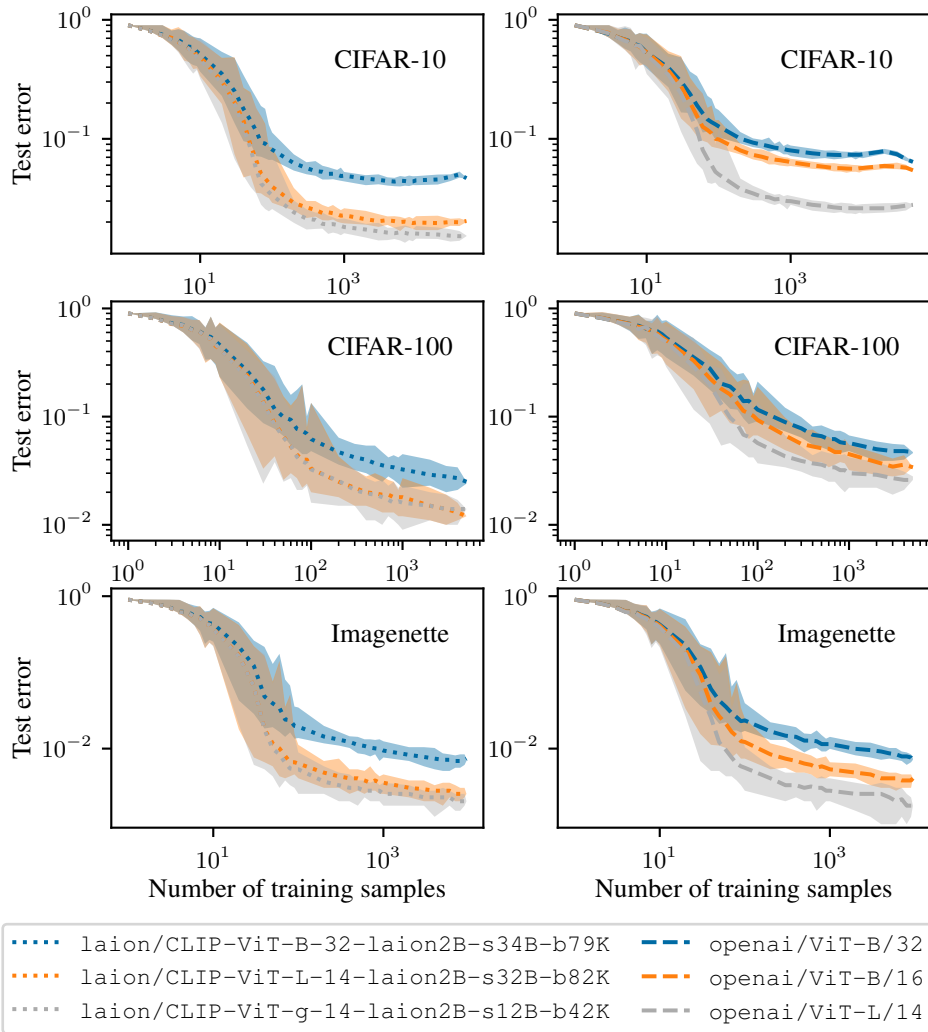


Figure D.3: Linear probe data-scaling of OpenAI and LAION CLIP models on CIFAR-10, SVHN, and ImageNette (Howard, 2022). Models consistently maintain relative ordering across datasets and n .

Another way of saying f_θ has bandlimit B is to say that

$$\min_{g \in S_B} \|f_\theta - g\|^2 = 0,$$

where the norm $\|\cdot\|$ is defined via $\|f\|^2 \triangleq \int_{x \in [0,1]^d} f(x)^2 dx$.

Main idea: In order to regularize f_θ towards having bandlimit B , we will add an approximate version of $\min_{g \in S_B} \|f_\theta - g\|^2$ to our loss. This approximation will be done via Monte-Carlo integration. It consists of the following steps:

1. Draw uniform i.i.d. samples x_1, \dots, x_m from $[0, 1]^d$.
2. Compute the vector

$$\mathbf{y} = \begin{bmatrix} f_\theta(x_1) \\ \vdots \\ f_\theta(x_m) \end{bmatrix}.$$

3. For each function ϕ in Φ_B , compute the vector

$$\mathbf{v}_\phi = \begin{bmatrix} \phi(x_1) \\ \vdots \\ \phi(x_m) \end{bmatrix}.$$

Then combine all the \mathbf{v}_ϕ into a matrix \mathbf{V}_B in the following manner:

$$\mathbf{V}_B = \begin{bmatrix} | & & | \\ \mathbf{v}_{\phi_1} & \cdots & \mathbf{v}_{\phi_{|\Phi_B|}} \\ | & & | \end{bmatrix}.$$

The matrix \mathbf{V}_B has m rows and $|\Phi_B|$ columns.

4. Finally compute

$$\frac{1}{m} \cdot \min_{\mathbf{z}} \|\mathbf{V}_B \mathbf{z} - \mathbf{y}\|_2^2 \approx \min_{g \in S_B} \|f_\theta - g\|^2.$$

The left hand side is equivalent to the quantity

$$\frac{1}{m} \cdot \|\mathbf{V}_B \mathbf{V}_B^+ \mathbf{y} - \mathbf{y}\|_2^2,$$

where \mathbf{V}_B^+ is the Moore-Penrose pseudoinverse of \mathbf{V}_B .

The regularized optimization in Section 3.3 was performed on the minibatch loss

$$\frac{1}{\text{batch_size}} \sum_{i=1}^{\text{batch_size}} (f_\theta(x_i) - h(x_i))^2 + \frac{\lambda}{m} \cdot \|\mathbf{V}_B \mathbf{V}_B^+ \mathbf{y} - \mathbf{y}\|_2^2.$$

with `batch_size` = 256, $B = 2$, $m = 2 \times 10^4$, and $\lambda = 1$.

F BINARY GAUSSIAN CLASSIFICATION TOY MODEL

In this section, we analyze a simple classification problem which demonstrates cliff-learning.

We assume the underlying data distribution for $\mathbf{x} \in \mathbb{R}^d$ and $y \in \{\pm 1\}$ is

$$y \sim \text{Unif}(\{\pm 1\}), \quad \mathbf{x} \sim \mathcal{N}(y \cdot s \cdot \mathbf{e}_1, I_d),$$

where $s \geq 0$ is a hyperparameter representing the signal-to-noise ratio.

From this data distribution, we draw n i.i.d. training datapoints $\{(x_i, y_i)\}_{i=1}^n$. We will use this data to learn a linear classifier to predict y from \mathbf{x} . Our linear classifier will take the form

$$f_w(x) = \text{sign}(w^\top x).$$

We will learn our linear classifier using the following learning algorithm:

$$\hat{w} = \frac{1}{n} \sum_{i=1}^n y_i x_i. \quad (\text{F.1})$$

Note that a linear change of coordinates does not effect the performance of our learning algorithm. Thus the results of this section apply to the more general case when $x \sim \mathcal{N}(y \cdot \mu, \Sigma)$ for an arbitrary $\mu \in \mathbb{R}^d$ and positive definite Σ .

The toy model here is approximately a simplified version of the model in Sorscher et al. (2022a) – we model x as Gaussian instead of uniform over an ellipsoid. This makes a difference in low dimensions, but in high dimensions the two distributions are extremely close.

F.1 ANALYTIC ERROR ASYMPTOTICS

For a fixed w , the test error of f_w can be written as

$$\begin{aligned} \text{Err}(f_w) &= \mathbb{P}(f_w(x) \neq y) \\ &= \mathbb{P}(\text{sign}(w^\top x) \neq y) \\ &= \mathbb{P}(w^\top x \cdot y < 0) \\ &= \mathbb{P}(w^\top \mathcal{N}(s \cdot e_1, I_d) < 0) \\ &= \mathbb{P}(\mathcal{N}(s \cdot w_1, w^\top w) < 0) \\ &= \Phi\left(-\frac{s \cdot w_1}{\|w\|_2}\right), \end{aligned} \quad (\text{F.2})$$

where $\Phi(x) = \int_{-\infty}^x \frac{1}{\sqrt{2\pi}} e^{-t^2} dt$ is the cumulative distribution function of the standard normal distribution.

Plugging in the learning algorithm for \hat{w} in Equation (F.1) into Equation (F.2), we have that

$$\frac{s \cdot \hat{w}_1}{\|\hat{w}\|_2} \stackrel{d}{=} \frac{s^2 + \frac{s\epsilon}{\sqrt{n}}}{\sqrt{s^2 + \frac{2s\epsilon}{\sqrt{n}} + \frac{\epsilon^2 + \chi_{d-1}^2}{n}}}, \quad (\text{F.3})$$

where $\epsilon \sim \mathcal{N}(0, 1)$ is a standard normal random variable, χ_{d-1}^2 is a Chi-squared random variable with $d - 1$ degrees of freedom, and $\stackrel{d}{=}$ denotes equality in distribution.

From Equation (F.3), we get that for large n ,

$$\begin{aligned} \text{Err}(f_{\hat{w}}) &\stackrel{d}{=} \Phi(-s) + \frac{\Phi'(-s)}{2s} \cdot \frac{\chi_{d-1}^2}{n} + O\left(n^{-3/2}\right) \\ &\stackrel{d}{=} \Phi(-s) + \frac{e^{-s^2/2}}{\sqrt{8\pi}s} \cdot \frac{\chi_{d-1}^2}{n} + O\left(n^{-3/2}\right), \end{aligned} \quad (\text{F.4})$$

which means with high probability, $\text{Err}(f_{\hat{w}})$ decays as a power law in the number of training samples n , with an irreducible error of $\Phi(-s)$.

F.2 EMPIRICAL DATA-SCALING LAWS

In Figure F.1, we show the data-scaling of $\text{Err}(f_{\hat{w}})$ for various values of d and s . Empirically, we find that for large d , the scaling curve is extremely well approximated as

$$\text{Err}(f_{\hat{w}}) \approx \Phi\left(-\frac{s}{\sqrt{1 + \frac{d}{ns^2}}}\right). \quad (\text{F.5})$$

When d is small, $\text{Err}(f_{\hat{w}})$ has much higher variance, but Equation (F.5) is nonetheless a good approximation of the the median value of $\text{Err}(f_{\hat{w}})$.

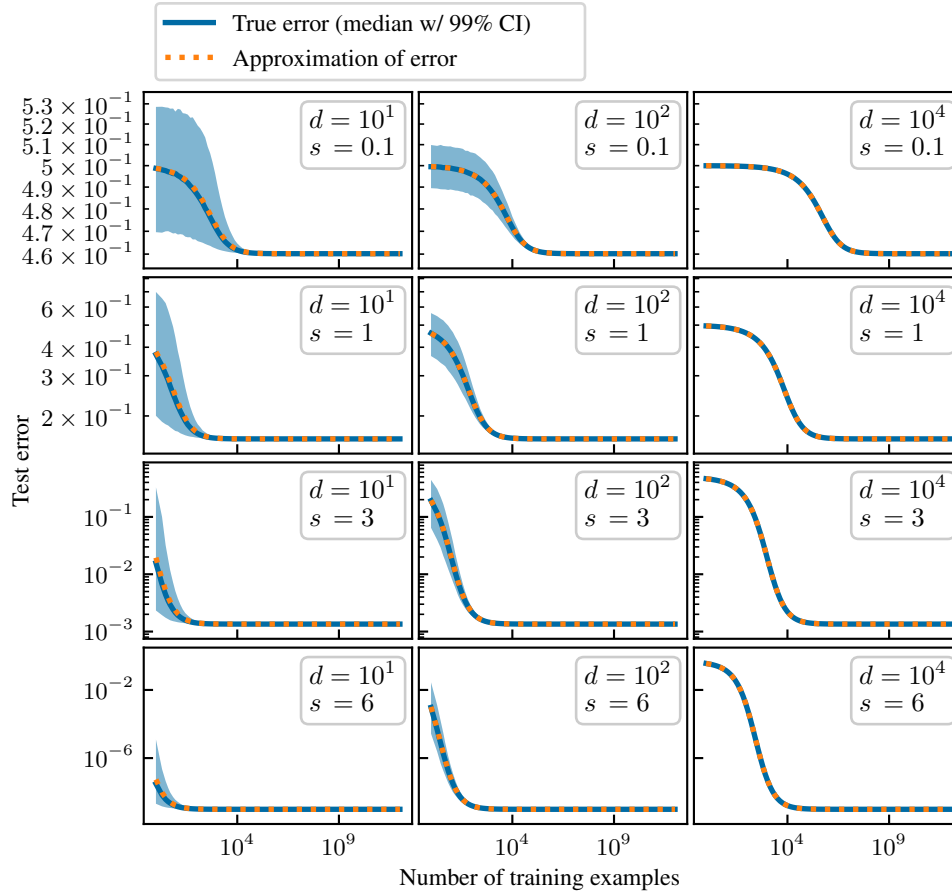


Figure F.1: Data scaling laws for the Gaussian toy model defined in Appendix F, showcasing a characteristic cliff shape. The blue lines denotes the median error of $f_{\hat{w}}$ over 10000 trials for various values of d and s , and shaded blue regions denote the 99% confidence intervals over those same trials. The orange lines are computed via Equation (F.5). Increasing s has the effect of decreasing the irreducible error, and increasing d reduces variance and shifts the entire curve to the right.